Magazine of Civil Engineering

ISSN 2712-8172

journal homepage: http://engstroy.spbstu.ru/

Research article

UDC 691.32

DOI: 10.34910/MCE.126.6

Corrosion-resistant concretes for coastal underground structures

S.V. Fedosov[1], ***O.V. Aleksandrova***[1], ***B.I. Bulgakov***[1], ***N.A. Lukyanova***[1] ✉, ***Q. Nguyen Duc Vinh***[2]

[1] *Moscow State University of Civil Engineering (National Research University), Moscow, Russian Federation*

[2] *Institute of Engineering and Technology – Hue University, Hue City, Vietnam*

✉ *galcevanadezda@mail.ru*

Keywords: underground concrete structures, concrete corrosion, active mineral additives, mathematical modelling, concrete-soil-liquid, strength, corrosion resistance and durability of concrete structures, diffusion of Ca^{2+} ions

Abstract. Introduction. The underground structures of the coastal zone in Vietnam are periodically flooded with seawater, which causes corrosion of concrete. Therefore, the aim of the study is to increase the corrosion resistance of coastal underground concrete structures by modifying the structure of concrete with a complex of mineral additives obtained mainly from local raw materials, including micro- and nanosilicon, fly ash from thermal power plants and finely ground white quartz sand. In addition, it requires development of a mathematical model describing the processes of mass transfer in conditions of liquid corrosion of concrete underground structures in coastal zone, to assess their durability. Methods. The development of concrete mixtures, the study of their properties and properties of concrete, were carried out in accordance with the requirements of current Russian and Vietnamese standards. Results and Discussion. The results of experimental studies confirmed the possibility of using local raw materials to create modifying additives and obtain corrosion-resistant concretes with high performance. It was found that with an increase in the content of white quartz sand in the concrete mixture, the compressive strength of concrete increased rapidly at an early age of hardening up to 7 days, after which its growth rate gradually decreased. Replacing 60 % of river sand with white quartz sand provided the highest compressive strength, axial tension and flexural tension of concrete, which can be explained by the fact that white quartz sand is finer than river sand, and this increases the density of the concrete structure. In addition, an increase in the density of concrete can be explained by a decrease in water absorption and an increase in resistance to sulfate corrosion with an increase in the content of white quartz sand in the concrete mixture instead of river sand, as well as with the introduction of 1–1.5 % nanosilicon. Conclusions. For the construction of underground structures in the coastal zone of Vietnam, we developed corrosion-resistant concrete compositions based on local raw materials with high strength characteristics and low water absorption. A mathematical model is proposed to solve the problem of determining the mass transfer of Ca^{2+} ions in the system "concrete structure – moist soil – coastal area" to control the processes of mass transfer during the corrosive destruction of concrete underground structures in coastal zones periodically flooded with seawater, in order to predict their operational durability.

Citation: Fedosov, S.V., Aleksandrova, O.V., Bulgakov, B.I., Lukyanova, N.A., Nguyen Duc Vinh, Q. Corrosion-resistant concretes for coastal underground structures. Magazine of Civil Engineering. 2024. 17(2). Article no. 12606. DOI: 10.34910/MCE.126.6

1. Introduction

Exposure of the concrete structure to aggressive soil layers with dry-wet cycles [1], repeated temperature and humidity changes, etc., causes serious damage to the structure and leads to reduced durability and service life of underground structures [2–5]. Therefore, the object of the study was corrosion-resistant concrete for coastal underground structures.

1.1. Factors affecting the durability of concrete in underground construction

The durability of concrete in underground structures is influenced by environmental factors, design and construction factors.

The design factors mainly include design form of the concrete structure, the thickness of the protective layer, and the strength of the concrete [6], while the construction factors mainly include method and construction process [7]. Environmental difficulties of underground construction are also a significant factor affecting the durability of concrete and its susceptibility to erosion and groundwater penetration. Concrete, which is constantly influenced by groundwater pressure, passes free water through itself, which can lead to the formation of cracks and the destruction of concrete structures [8]. The result of this process can be the biological decomposition and erosion of concrete material, the enrichment of the soil with minerals and the development of microorganisms that can actively multiply on the surface of concrete and contribute to its destruction. In difficult operating conditions, when exposed to factors such as soil pressure and groundwater pressure, concrete undergoes significant compression or stretching, and an increase in stress significantly reduces its durability. In a complex stressed environment with such factors as soil pressure and seepage pressure, concrete will experience severe compression or tensile stress, an increase in stress will lead to a decrease in durability. The ions Cl^- or SO_4^{2-} in moist soil accelerate the erosion of concrete and form an electrochemical erosion environment [9]. During the construction of various underground structures, one of the primary missions is to guarantee the durability and reliability of concrete structures [10], as well as the resistance to subterranean and aggressive water, which, in turn, should be taken into an account when developing concrete compositions.

1.2. Coastal groundwater systems

Coastal regions are interface zones between land and ocean, which are affected by both marine and terrestrial processes [11]. The coastal area is quite an ill-defined concept, for which various definitions were proposed [12]. For example, it can be understood as a contiguous and hydro-logically connected land area along the coast and below 10 m above sea level [13].

Underground water in coastal aquifers is usually a mixture of fresh and seawater. Since the salinity of seawater is higher than compared to recharge of freshwater of groundwater sources, small amounts of seawater can prevail in chemical composition [14, 15]. Adding one percent of seawater to freshwater with 0.1 g/l of chloride increases the chloride concentration by nearly three times; supplementing five percent of seawater content increases the salinity of the source fresh water to more than 1 g/l [16]. Superimposed on mixing effects are the changes in the composition of groundwater in coastal aquifer systems due to chemical processes. Rising sea levels can impact coastal aquifer systems in several ways [17]. The boundary between seawater and fresh groundwater is pushed further inland, which leads to an increase in the seawater penetration. There is further migration of seawater upstream along river channels in coastal estuaries, which then affects the salinity of adjacent groundwater [18, 19].

The durability of concrete directly affects the service-life of underground concrete structures [20]. With the speeding up pace of urban construction and the scale of urbanization, the development of urban underground space in Vietnam became one of the important ways for the sustainable development of urban infrastructure [21]. However, underground concrete structures are exposed to the groundwater, which affects the characteristics of the concrete structure, such as impermeability and corrosion resistance [22]. Currently, at the early stages of underground construction in an underground humid environment, serious problems related to durability have arisen, which leads to subsequent repairs that will require a lot of labor and material resources. Understanding the mechanism of concrete quality degradation as a result of exposure to aggressive environmental factors [23] is important to design the composition of corrosion-resistant concrete for underground structures in coastal areas, which was the main purpose of this study [24].

To achieve this goal, it is necessary to solve the following two main tasks:

– to improve the physical and mechanical properties and corrosion resistance of concrete intended for the construction of underground structures in the coastal zone periodically flooded with

seawater, by modifying its structure, to develop a complex of active mineral additives, using mainly local raw materials for the southern region of Vietnam;

– to develop a mathematical model of the mass transfer process under conditions of liquid corrosion of concrete, taking into account the influence of the soil of the coastal zone.

2. Methods

2.1. Materials

The following raw materials were used to produce samples from corrosion-resistant concrete:

2.1.1. Mineral binding material

Mineral binding material: sulfate-resisting Portland cement PCsr40 (type 5) manufactured by Luks Cement Limited (Vietnam) in accordance with TCVN 6067 and GOST 22266 standards. C_3A content was 2.49 % and $C_4AF + 2C_3A$ content was 21.23 %. Initial and final setting time were 170 and 213 min., respectively. Compressive strength at the age of 3 and 28 days of normal hardening – 25.7 and 46.5 MPa, respectively. Sulfate expansion after 14 days is 0.016 % (Tables 1 and 2).

Table 1. Chemical composition of cement.

SiO_2	Al_2O_3	Fe_2O_3	CaO	MgO	K_2O	Na_2O	TiO_2	BaO	SO_3	L.O.I.*
20.59	3.77	5.06	62.12	1.72	0.63	0.14	0.12	1.89	2.0	1.96

* Loss on ignition

Table 2. Properties of cement.

Specific surface, m^2/kg	Density, g/cm^3	Average particle size, μm
363.3	3.15	14

Coarse aggregate: crushed granite rock from Ga Loi quarry (Vietnam), two size fractions of the coarse aggregates including size range 5–10 mm and 10–20 mm were mixed follow proportions 40:60 % by mass, density of 2.68 g/cm^3, water absorption 0.5 %, average strength 105.6 MPa, according to standards TCVN 7570 and GOST 8267-93*.

Fine aggregates included (1) natural river sand (Rs) of the Huong River (Vietnam) with fineness modulus (M_k) of about 3.0, density of 2.65 g/cm^3, water absorption 2 %; and (2) whiter quartz sand (Qs), with average particle size of 0.1÷1.8 mm. It is also known as interior field sand or natural whiter sand, according to standards TCVN 10796 and GOST 8736.

Mineral admixtures: silica fume (SF) as mineral admixture in dry densified form obtained from Sikacrete® PP1 – Sika limited Vietnam, with particle size < 0.1 μm and density approx. 2.15 g/cm^3 conforming to TCVN 8827 and GOST P 56592 standards. Class F fly ash (FA) of thermal power plants Pha Lai, Vietnam, conforming to TCVN 10302 and GOST 25818 standards. Finely ground quartz powder (Qp) milled from natural whiter sand with average particle size from 5 to 95 μm plays a role of micro filler. Nanodisperse silica (SiO_2), which was the product of process synthesis from whiter quartz sand (Vietnam). All admixtures are presented in Tables 3 and 4.

Table 3. Chemical composition of mineral additives.

Name of additive	Components, % by weight							
	SiO_2	Al_2O_3	Fe_2O_3	CaO	MgO	K_2O	Na_2O	TiO_2
Finely ground quartz powder	99.7	0.046	0.043	0.054	0.038	0.0068	0.023	0.045
Silica fume	92.48	0.86	1.91	0.32	0.85	1.22	0.38	–
Fly ash (Class F)	57.43	24.05	6.06	0.68	0.97	3.60	0.27	0.7
Nanodisperse silica (SiO_2)	99.95	–	0.013	0.037	–	–	–	–
Name of additive	Components, % by weight							
	P_2O_5	ZrO_2	Cr_2O_3	CuO	ZnO	BaO	SO_3	L.O.I.*
Finely ground quartz powder	–	–	–	–	–	–	–	0.044
Silica fume	–	–	–	–	–	–	0.3	1.68
Fly ash (Class F)	0.11	0.03	0.02	0.02	0.03	–	0.3	5.74
Nano - SiO_2	–	–	–	–	–	–	–	–

Table 4. Properties of mineral additives.

Properties / Mineral additives	Specific surface, m^2/kg	Density, kg/m^3	Particle size, μm
Finely ground quartz powder	~ 250	2670	5–95
Silica fume	15000 – 30000	2150	< 0.1
Fly ash (Class F)	~ 9600	2410	1–8
Nano – SiO_2	139000	2330	$(10–50)10^{-3}$

Chemical admixture: polycarboxylate superplasticizer (SP) Sika® ViscoCrete®-151 with density of 1.075–1.095 kg/l and pH value of 4.0÷6.0 conforming to TCVN 8826 and GOST 24211 standards.

2.2. Research methods

2.2.1. Design of concrete mix compositions

The concrete mixes were developed using existing composition design methods, namely, TCVN 10306 and GOST 27006 standards. At the beginning of the experiment, the composition of concrete mixture for concrete with the average strength of 80 MPa was obtained without considering the addition of any mineral and chemical admixtures and was treated as a basic mix proportion. The control concrete mixture composition (admixture-free) is presented in Table 5.

Table 5. Concrete mixture proportions.

Materials	Quantity material	Absolute volume, m^3	Mix proportion
Water, kg/m^3	156	$156/10^3$	0.284
Cement, kg/m^3	550	$550/3.15=174.6/10^3$	1
Crushed rock aggregate, kg/m^3	1088	$1088/2.68=405.97/10^3$	1.98
Natural river sand, kg/m^3	654	$654/2.65 = 247/10^3$	1.19
Entrained air, %	2	$20/10^3$	-
Superplasticizer Sika®Viscocrete® -151, l/m^3	9.9	$9.9/1.075=9.2/10^3$	0.018
Sum total		$1000/10^3$	4.472

2.2.2. Ultrasonic pulse velocity method

The 100×100×100 mm cubic samples were tested using ultrasonic pulse velocity (UPV) on the 28th day of curing according to TCVN 9357 and GOST 17624-2021 standards.

Ultrasonic velocity was measured in a direct way, through cubic samples and between two parallel sides. The pulse velocity measuring device uses a transmitting transducer to send a compression wave into the concrete and a receiving transducer at a distance of L, which receives a pulse sent through the concrete from another point. The display of the device shows the time T required for the pulse to pass through the concrete. Ultrasound velocity (V), m/s, is calculated by the formula:

$$V = \frac{L}{T} \cdot 10^{-3},$$

where T is the actual time passage of the ultrasonic pulse through medium, s; L is the distance between the centers of the transducer installation zones (sounding base), mm.

The test method for pulse velocity passing through concrete was standard. The device used to determine the ultrasonic pulse velocity is the TICO concrete ultrasonic detector was developed by Proceq in Zurich, Switzerland. The device can calculate and evaluate the functions of concrete homogeneity, crack depth, modulus of elasticity, and concrete strength [25].

2.2.3. Workability of concrete mix

The workability of concrete mix was determined in conformity with TCVN 3106 and GOST 10181 standards. The workability of concrete mixes is checked and evaluated by filling capacity and resistance of segregation. TCVN 12209 and GOST R 57812 standards pose the main requirements for the flowability of concrete mixtures: 550 mm ≤ SF ≤ 750 mm; 3 s ≤ T500 ≤ 25 s; 0 ≤ PA ≤ 50 mm; 0 mm ≤ Δh ≤ 25 mm.

2.2.4. Determination resistance to leaching corrosion of concrete samples

The corrosion resistance of concrete in aggressive environments was assessed according to TCVN 9346:2012 and Russian State Standard GOST 31384-2017. Three control and three main samples for each aggressive environment from each concrete composition on cube samples of 150×150×150 mm or 100×100×100 mm in size were assessed at the age of 28 days of normal hardening.

2.3. Chemical composition of groundwater in coastal regions of South Vietnam

Over the past two decades, like any part of the world, Southeast Asia has witnessed climate change with increasing numbers of extreme heat waves, tropical storms with, heavier rains of increasingly terrible and unpredictable intensity. The major impacts of climate change leading to many environmental changes have had a severe impact on the lower Mekong basin: it is one of the most vulnerable regions to climate change, which faces land subsidence, saltwater intrusion, extreme drought, riverbank and coastal erosion and sea level rise. Across the Greater Mekong region, temperatures have risen by 0.5 to 1.5 °C in the past 50 years and continue to rise. By the end of the century, higher sea levels in the Mekong Delta may inundate about 1.4 million ha threatening the region's coastal communities.

Salinization of surface waters. Various sources contribute to the salinization of surface waters. The penetration of seawater into rivers, the migration wedge of saltwater to land due to differences in density, are the main sources of salinity in the mouths of rivers with open water. Thus, in these regions, the salinity of surface waters is closely related to salt deposition and its distribution in shallow groundwater [26]. The study area is located in the upper and lower reaches of the rivers along the Hậu River (Bassac River) and Mekong River of southern Vietnam given in the study by H. Sato et al. [27]. The characteristics of ionic compositions and analytical data of dissolved ions are given Fig. 1 showing a statistical analysis of the chemical characteristics of shallow groundwater samples.

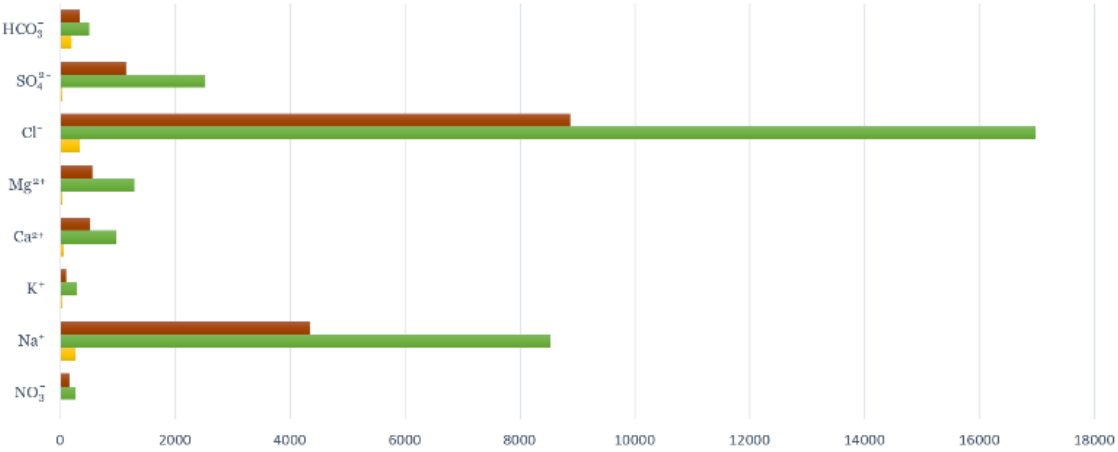

	NO_3^-	Na^+	K^+	Ca^{2+}	Mg^{2+}	Cl^-	SO_4^{2-}	HCO_3^-
Medium, mg/l	153.26	4331.75	102.74	510.5	554.92	8876.4	1143.56	341.2
Maximum, mg/l	264.18	8535.8	278.81	970.48	1290.06	16970.5	2511.29	502.19
Minimum, mg/l	12.38	266.85	22.8	60.21	37.67	345.71	26.82	195.87

Figure 1. Chemical characteristics of shallow groundwater.

2.4. Mathematical model

In order to predict the corrosion resistance of concrete structures, it is necessary to develop a mathematical model describing the processes of diffusion-kinetic penetration of aggressive seawater salts of coastal zones into soil bases and enclosing structures. The evaluation of the effect of different service conditions on the durability of reinforced concrete structures in underground engineering of coastal regions is to be made by using mathematical modeling and numerical experiments based on them. Several mathematical models of predicting concrete corrosion process in different corrosion environments have been developed and applied in practice. For example, the mathematical models by S.V. Fedosov and a few others [28].

The effectiveness of computational methods using a new mathematical model for predicting the corrosion process of concrete and reinforcement in underground structures has been demonstrated through the results obtained for each specific work. The results obtained from both models theoretical and experimental give equivalent values. The obtained mathematical relation help to solve the inverse problem with using available experimental data, it is possible to predict the numerical value of free $Ca(OH)_2$ by thickness of the structure. Below is a mathematical model of mass transfer for the processes of liquid corrosion of cement concretes, taking into account the influence of the coastal region soil. The "concrete

structure – moist soil – seawater area" system can be represented by two plates of non-limiting contacts. Each plate is characterized by its dimensions (a concrete wall of thickness δ_1, on the right side, was in contact with a moist soil layer of thickness δ_2 and the soil is in contact with saline water) and properties (Fig. 2).

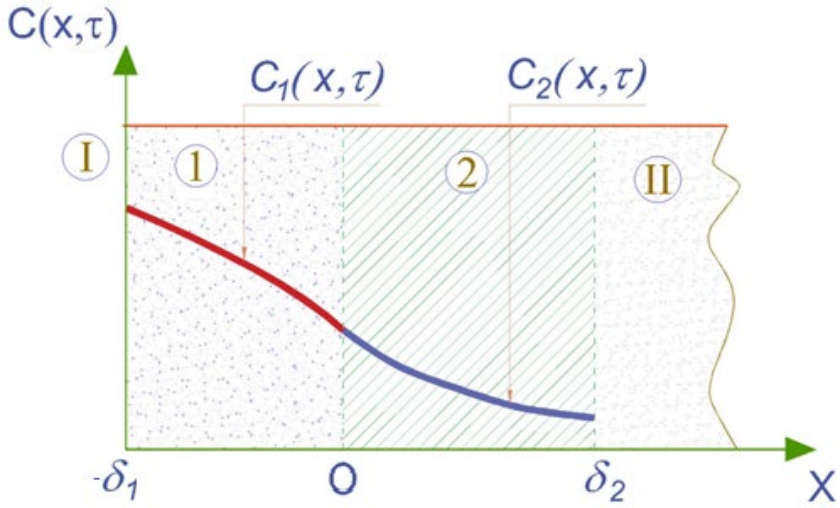

Figure 2. Mass transfer model: I is indoor environment, II is marine water area; 1 is concrete structure, 2 is moist soil; δ_1 is thickness of structure, δ_2 is the size of soil.

A mathematical model of mass transfer in an unlimited two-layer plate can be represented as a system of partial differential equations with combined boundary conditions of the second kind at the external boundaries of the system and of the fourth kind at the boundary of concrete with soil. The mathematical model of non-stationary mass transfer processes in the "reinforced concrete – soil – coastal water" system should be a solution of two boundary problems of mass conductivity with nonlinear boundary conditions in the concrete structure and coastal soil massif.

A feature of these problems will be the use of boundary conditions of the combined type: second kind on the inner surface of the reinforced concrete structure; second to third kind on the border of the soil with the water area, and fourth kind on the border of the structure and the soil.

There are mathematical expressions describing these boundary value problems in a dimensionless form below.

– Mass conduction differential equations:

$$\frac{\partial Z_1(\overline{x},Fo_m)}{\partial Fo_m}=\frac{\partial^2 Z_1(\overline{x},Fo_m)}{\partial \overline{x}^2},\ Fo_m>0;\ \ -1\le\overline{x}\le 0; \tag{1}$$

$$\frac{\partial Z_2(\overline{x},Fo_m)}{\partial Fo_m}=\frac{\partial^2 Z_1(\overline{x},Fo_m)}{\partial \overline{x}^2}\cdot K_k,\ Fo_m>0;\ \ 0\le\overline{x}\le K_\delta. \tag{2}$$

– Initial conditions that determine the fields of mass transfer potentials at the time taken as the initial $(Fo_m=0)$,

$$Z_1(\overline{x},Fo_m)\Big|_{Fo_m=0}=Z_{1,0}(\overline{x}); \tag{3}$$

$$Z_2(\overline{x},Fo_m)\Big|_{Fo_m=0}=Z_{2,0}(\overline{x}). \tag{4}$$

The following designations are adopted here:

$$\overline{x}=\frac{x}{\delta_1},\ \ Fo_m=\frac{k_1\tau}{\delta_{\delta 1}^2}; \tag{5}$$

$$Z_1(\overline{x},Fo_m)=\frac{C_{1,0}-C_1(x,\tau)}{C_{1,0}},\ \ Z_2(\overline{x},Fo_m)=\frac{C_{2,0}-C_2(x,\tau)}{C_{2,0}}; \tag{6}$$

$$K_\delta = \frac{\delta_2}{\delta_1},\ K_k = \frac{k_2}{k_1}, \tag{7}$$

where $C_1(x,\tau)$ is concentration of "free" $Ca(OH)_2$ determined by CaO content in concrete at time (τ) evaluated at an arbitrary point of co-ordinate (x), kg CaO·kg^{-1} of concrete; $C_2(x,\tau)$ is concentration of "free" $Ca(OH)_2$ determined by CaO content in the soil layer at time (τ) at an arbitrary point of co-ordinate (x), kg CaO·kg^{-1} of solid; $k_{1,2}$ are mass conductivity coefficients, m^2/s; δ_1 is thickness of concrete structure, m; δ_2 is thickness of soil layer, m.

– Boundary conditions of the second on the inner surface of a reinforced concrete structure:

$$\frac{\partial Z_1(|-1|, Fo_m)}{\partial \overline{x}} = 0. \tag{8}$$

– Boundary conditions of the fourth kind at the point of contact of two solid bodies:

$$Z_1(\overline{x}, Fo_m)\big|_{\overline{x}=0} = Z_2(\overline{x}, Fo_m)\big|_{\overline{x}=0}; \tag{9}$$

$$\left.\frac{\partial Z_1(\overline{x}, Fo_m)}{\partial \overline{x}}\right|_{\overline{x}=0} = N \left.\frac{\partial Z_2(\overline{x}, Fo_m)}{\partial \overline{x}}\right|_{\overline{x}=0}, \tag{10}$$

where $N = \frac{\rho_2}{\rho_1}\cdot\frac{k_2}{k_1}\cdot\frac{1}{m}$ is a coefficient that takes into account the characteristics of phases.

– Boundary conditions of the second kind at the boundary of the soil massif and the coastal water area:

$$\frac{\partial Z_2(K_\delta, Fo_m)}{\partial \overline{x}} = Ki_H^*, \tag{11}$$

where $Ki_H^* = \frac{\rho_H\cdot\rho_1\cdot m\cdot K_\delta}{\delta_2\cdot\rho_2\cdot k_2\cdot C_0}$ is Kirpichev criterion for mass transfer.

The solution of these boundary value problems was obtained by the method of Laplace integral transformations [28].

The general solution of the mass conductivity problems describing the dynamics of concentration fields has the form [29]:

$$\begin{aligned} Z_1(\overline{x}, Fo_m) = \\ = \frac{1}{1+NK_kK_\delta}\left\{1 - NK_\delta + Ki_H^*\left[Fo_m + \frac{(1-\overline{x})^2}{2} + \varphi(K_k, N, K_\delta)\right]\right\} + 2\sum_{m=1}^{\infty}\frac{1}{\mu_m^2\psi_1/(\mu_m)}\cdot \\ \cdot\left\{\mu_m \sin\mu_m\left[\cos(\mu_m\overline{x})\cos\left(\mu_m\sqrt{K_k}K_\delta\right) - \sqrt{K_k}K_\delta\sin(\mu_m\overline{x})\sin\left(\mu_m\sqrt{K_k}K_\delta\right)\right] - \right. \\ \left. - \frac{N}{\sqrt{K_k}}\cos(\mu_m(1+\overline{x}))\right\}\exp\left(-\mu_m^2 Fo_m\right); \end{aligned} \tag{12}$$

$$Z_2\left(\bar{x},Fo_m\right)=\frac{1}{1+NK_kK_\delta}\cdot$$

$$\cdot\left\{1-NK_\delta+Ki_H^*\left[\bar{x}-Fo_mK_kK_\delta\right]+NKi_H^*\left(\varphi\left(K_k,N,K_\delta\right)-\frac{1+K_k\bar{x}^2}{2}\right)\right\}-$$

$$-2\sum_{m=1}^{\infty}\frac{\sin\left(\mu_m\sqrt{K_k}\cdot K_\delta\right)}{\mu_m^3\sqrt{K_k}\psi_1'\left(\mu_m\right)}\left\{\mu_m\sin\mu_m\cos\left[\mu_m\sqrt{K_k}\left(K_\delta-\bar{x}\right)\right]-\right. \quad (13)$$

$$-\frac{\mu_m}{\sqrt{K_k}}\sin\left(\mu_m\sqrt{K_k}K_\delta\right)\left[N\cos\mu_m\cos\left(\mu_m\sqrt{K_k}\bar{x}\right)+\frac{1}{\sqrt{K_k}}\sin\mu_m\sin\left(\mu_m\sqrt{K_k}\bar{x}\right)\right]+$$

$$\left.+Ki_H^*\left[N\cos\mu_m\cos\left(\mu_m\sqrt{K_k}\bar{x}\right)+\frac{1}{\sqrt{K_k}}\sin\mu_m\sin\left(\mu_m\sqrt{K_k}\bar{x}\right)\right]\right\}\exp\left(-\mu_m^2K_kFo_m\right),$$

where μ_m is roots of the characteristic equation,

$$\mathrm{tg}\mu_m=N\sqrt{K_k}\,\mathrm{tg}\left(\mu_m\sqrt{K_k}K_\delta\right); \quad (14)$$

$$\varphi\left(K_k,N,K_\delta\right)=\frac{1+K_kK_\delta\left(3K_\delta+3N+NK_kK_\delta^2\right)}{6\left(1+NK_kK_\delta\right)}; \quad (15)$$

$$J=\int_0^1 Z_{1,0}\left(\xi\right)\cos\left[\mu_m\left(1-\xi\right)\right]d\xi. \quad (16)$$

The interpretation of the values of the obtained equations is given in [29]. Fig. 3 illustrates the dependence of dimensionless concentrations on the Kirpichev mass transfer criterion [30]. With increasing (ρ) of the Kirpichev mass transfer criterion, large gradients (α) of concentrations appear.

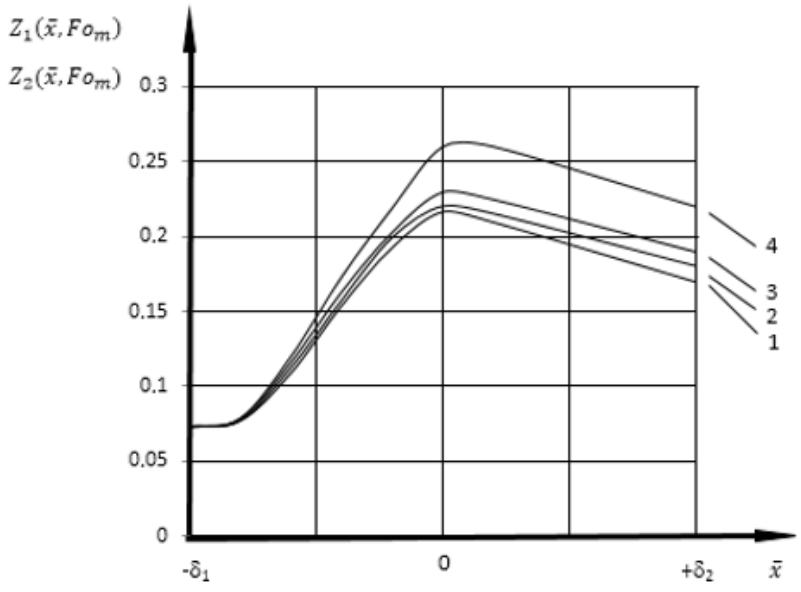

Figure 3. Diagram of dimensionless concentrations in the thickness of concrete and soil at K_k = 1; K_δ =0.1; Fo_m = 1 with different values of Ki_H^*: 1 – 0.5; 2 - 1; 3 – 1.5; 4 – 2.

The successful design of concrete composition with high anticorrosive properties is possible if the effect of aggressive environmental factors during the operation of concrete and reinforced concrete products and structures is taken into account.

3. Result and Discussion

3.1. Technological properties of concrete mixtures

Seven compositions of concrete mixes were prepared: a control mixture (100 % river quartz sand) and six mixtures containing white quartz sand in various proportions. Fine aggregate (river sand) was replaced by white quartz sand by weight. The proportion of the replaced fine aggregate varied from 40 % to 100 % in increments of 20 %. The influence of white quartz sand on the mechanical properties, corrosion resistance of concrete and reinforcing steel in concrete was investigated. The compositions of concrete mixtures are presented in Table 6.

Table 6. Compositions of concrete mixtures, kg/m³.

Mixture No.	Cementitious materials (B), kg/m³					Concrete aggregate, kg/m³					Water	SP	(W+SP)/B
	Cement	SF	FA	Nano SiO_2		Coarse aggregate	Fine aggregate						
							Rs		Qs	Qp			
	kg	kg	kg	%	kg	kg	kg	%	Kg	kg	kg	l	–
5aS0	357.5	27.5	165	–	–	1088	592.3	–	–	104.5	127.6	9.9	0.25
5aS1	352.0	27.5	165	1.0	5.5	1088	592.3	–	–	104.5	127.6	9.9	0.25
Q40	357.5	27.5	165	–	–	1088	355.4	40	236.9	104.5	127.6	9.9	0.25
Q60	357.5	27.5	165	–	–	1088	236.9	60	355.4	104.5	127.6	9.9	0.25
Q80	357.5	27.5	165	–	–	1088	118.5	80	473.8	104.5	127.6	9.9	0.25
Q100	357.5	27.5	165	–	–	1088	–	100	592.3	104.5	127.6	9.9	0.25
QS1.0	352.0	27.5	165	1.0	5.5	1088	–	100	592.3	104.5	127.6	9.9	0.25
QS1.5	349.3	27.5	165	1.5	8.25	1088	–	100	592.3	104.5	127.6	9.9	0.25

Mixture designations: No. 5aS0 is the control mixture in which natural river sands (with content 100 % by weight of fine aggregate) were used as a fine aggregate. Mixtures No. Q40, No. Q60, No. Q80, and No. Q100 contain white quartz sand in the amount of 40, 60, 80 and 100 % by weight of natural river sand, respectively; No. QS1.0 and No. QS1.5 – mixtures contain 100 % white quartz sand and nano-SiO_2 content of 1 and 1.5 %, respectively.

After curing, the cubes were used to determine the total compressive load taken by concrete at different ages including 3, 7, 14, 28, 365, and 450 days of age. Compression testing machine Matest model C089-17N with the capacity of 3000 kN was used for compressive tests of all specimens. Cylinders and beams were tested on a testing machine up to 600 kN, at the age of 28 days to determine the splitting tensile and flexural strength of concrete. The results of the tests for the spreading of the concrete mixture are shown in Table 7, the tests of concrete mixtures are shown in Fig. 4.

Table 7. Results of tests for the spreading of concrete mixtures.

Mixture No.	Spreading diameter, SF	Time, T_{500}	J-Shaped ring		Separation
			ΔH	SF_J	
	mm	s	mm	mm	Yes/No
5aS0	560	8.0	22	500	No
Q40	620	7.5	17	580	No
Q60	690	6.0	15	700	No
Q80	730	5.0	14	695	No
Q100	760	3,7	13	730	No
QS1.0	740	4.5	14	705	No
QS1.5	700	5.0	16	660	No

According to the observations during the experiment and results obtained from tests in Table 7 following conclusions can be drawn: 1) segregation was not observed in any of the studied concrete

mixtures; 2) the spreading diameter (slump flow) of the No. Q100 mixture is 760 mm, relegate to Class SF2, high flowability according to TCVN 12209 standard; 3) the result of T500 time (a measure of viscosity) of the No. Q100 mixture is 3.7 s, in the range of 3 to 25 s, which meets the requirements; 4) the result of ΔH (inside and outside) is 13 mm of the No. Q100 mixture in the range is 0 to 25 mm, which meets the requirements; 5) the passing ability result of the No. Q100 mixture is PA = SF – SFJ = 30 mm, which corresponds to Class PA1 meeting the requirements.

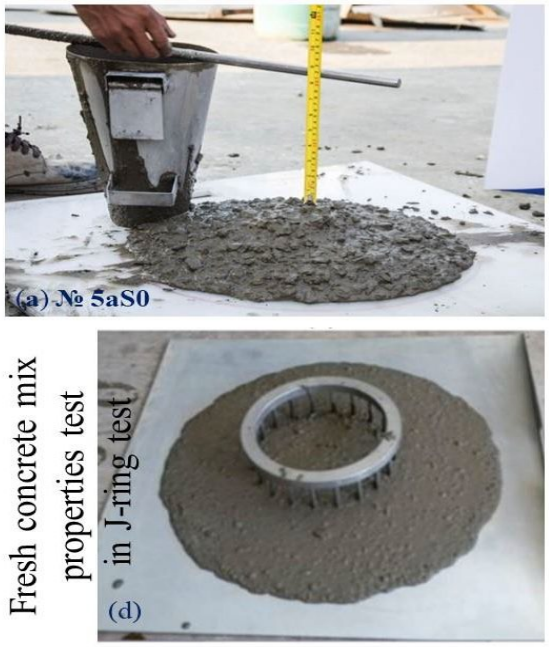

Figure 4. Tests for the workability of concrete mixtures: (a) Slump cone test or spreading (slump flow) test for concrete; (d) Limited spread measurement test.

3.2. Determination of mechanical characteristics of concrete

For concretes obtained as a result of hardening of the investigated concrete mixtures, compressive strength was determined at the age of 3, 7, 28, 356, and 450 days and the tensile strength in the axial direction, the bending strength at the age of 28 days according to GOST 10180 standard. The obtained test results are presented in Fig. 5 and 6.

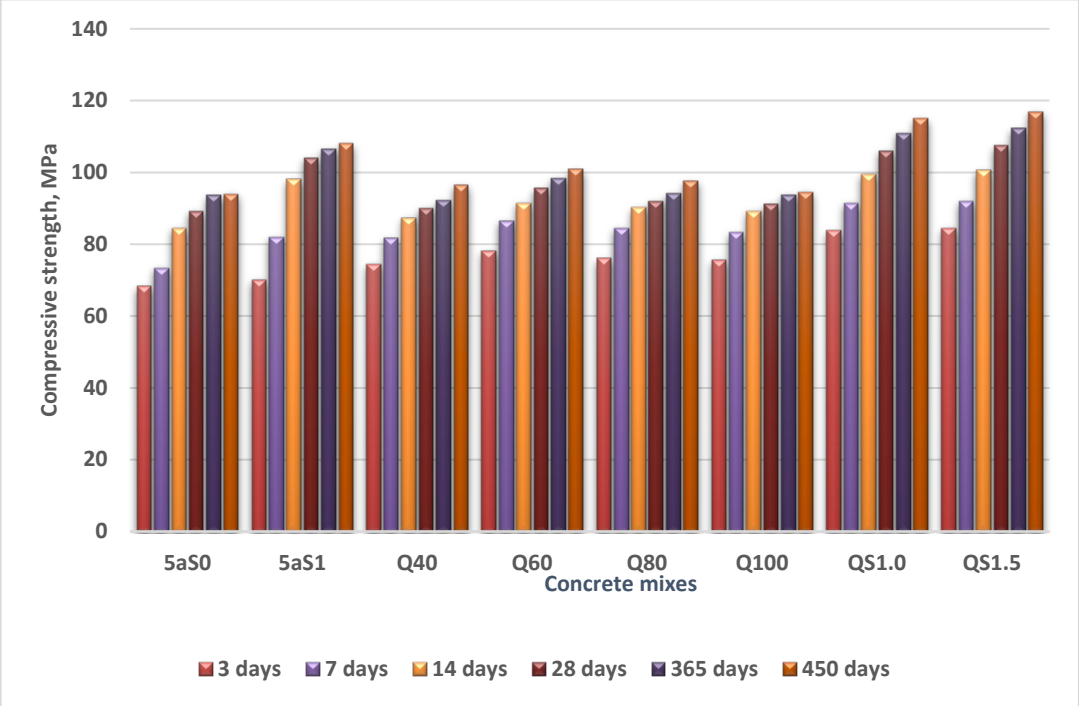

Figure 5. Change in the compressive strength of concrete at different curing ages.

The main purpose of the study was to utilize white quartz sand as an alternative for natural river sand in concrete production, and not to enhance the strength characteristics of concrete. However, the received experimental results showed that when white quartz sand was used as a fine aggregate instead of river sand in the concrete mixture, an increase in strength was observed at all substitution ratios. Fig. 5 shows that with an increase in the amount of white quartz sand in concrete, compressive strength develops rapidly at an early age, namely from 3 to 7 days and it's growth is gradually slowing down at a later age.

In addition, concrete samples containing white quartz sand showed higher compressive strength than the No. 5aS0 control sample during all hardening periods. In these results, at the age of 3 days, compressive strength of the concrete containing white sand in the amount of 40, 60, 80, and 100 % (by weight of river sand) reached the compressive strength values of 74.5, 78.2, 76.0, and 75.5 MPa, respectively. These values exceed the compressive strength of the control sample (No. 5aS0) with a value of 68.2 MPa. With an amount of white quartz sand equal to 60 %, concrete compressive strength has the highest values at different curing ages. The results show that 60 % replacement of river sand by white quartz sand provided optimal strength. No. Q60 mixtures showed higher compressive strength compared to mixtures No. 5aS0 (control mixture), No. Q40, No. Q80, and No. Q100 with the values of 7.2 %, 6.1 %, 3.8 %, and 4.7 %, respectively, and this difference in strength is comparatively high. The increase in compressive strength of concrete mixtures containing white quartz sand compared to the control mixture (river sand) is explained by the fact that white sand is finer than river sand, which leads to an improvement in the particle packing density of the concrete mix.

Compared to No. 5aS0 reference mixture, the No. Q100 mixture containing 100 % white quartz sand showed 9.7 %, 12.0 %, 5.2 %, 2.3 %, 0.2 %, and 0.5 % higher compressive strength at the age of 3, 7, 14, 28, 356 and 450 days, respectively. This can be explained by the fact that certain properties of river sand, such as porous structure and uneven intensity, differences in the physicochemical properties of fine aggregate particles in its composition, and high water absorption lead to water demand for concrete mixes, which causes a reduction in concrete strength. Another possible factor is the presence of impurities, such as clay content, organic impurities, small plant waste, silt, as well as unequal strength and structure of aggregate particles from river sand, which creates air voids in concrete. This reduces the specific density of the material, as result a significant decrease in concrete strength.

Split-tensile and flexural strength at the age of 28 days. In Fig. 6 were summarized the results obtained by tests of tensile and flexural strength for various concrete compositions at the age of 28 days. The change in split-tensile and flexural strength of concrete containing white quartz sand was similar to one in compressive strength. Compared to the No. 5aS0 reference sample, the No. Q60 mixtures showed higher split-tensile and flexural strength values of 7.26 MPa and 9.78 MPa, respectively. The average results of the three 100×200 mm cylinders that were used to test split tensile strength are shown in Fig. 6. The 28-day split tensile strength showed a decrease of 0.55 %, 0.97 %, and 1.66 % corresponding to mixtures No. Q40, No. Q80, and No. Q100, and an increase of 0.6 % for the mixture No. Q60 compared to reference mixture No. 5aS0 (tensile strength value is 7.22 MPa).

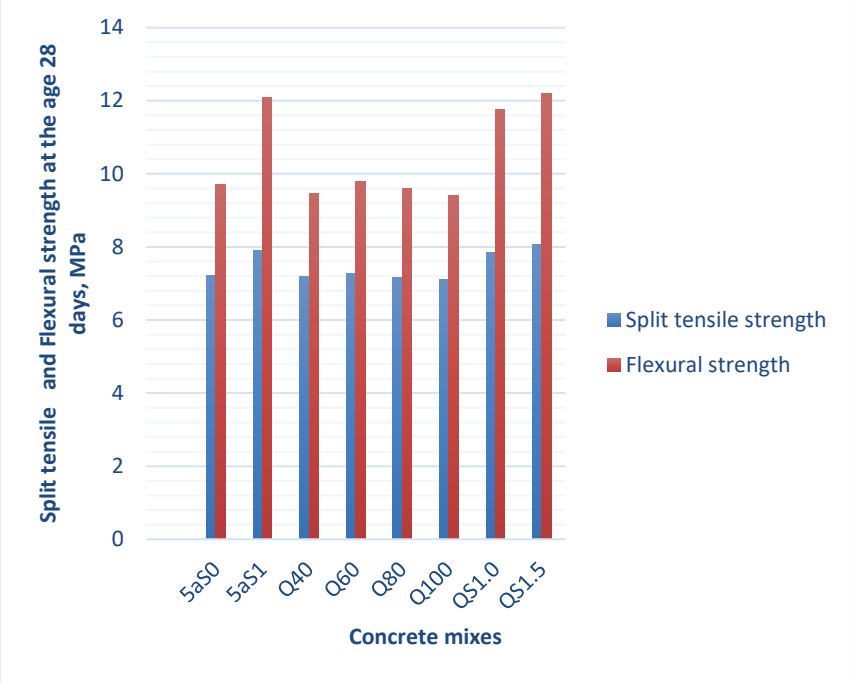

Figure 6. Split tensile strength and flexural strength of concrete at the age of 28 days.

The results of the flexural strength tests are presented in Fig. 6, the 28-day flexural strength showed a decrease of 2.68 %, 1.13 %, and 2.16 % for mixtures No. Q40, No. Q80, and No.Q100 and an increase of 0.72 % for mixtures No. Q60 compared to reference mixture No. 5aS0 (tensile strength value is 9.71 MPa). The optimal composition for replacing natural river sand with white quartz sand is of Q60 mixes composition, which showed the greatest strength at the age of 28 days.

Water absorption was determined according to TCVN 3113 and GOST 12730.3 standards. Tests were carried out on cube samples measuring 100x100x100 mm. The samples were tested after 28 days of curing. The average value of three samples was indicated as water absorption for each concrete mixture. The test results are presented in Fig. 7.

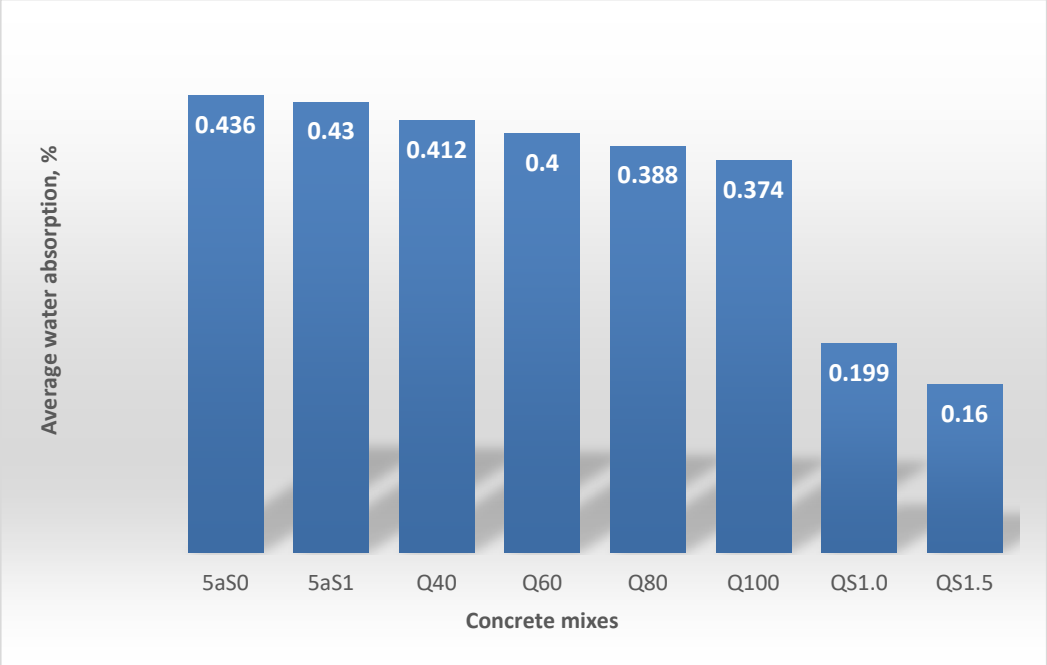

Figure 7. Effect of white quartz sand and Nano-SiO_2 on water absorption of concrete.

The water absorption rate of the concrete reduced as the white quartz sand content in concrete mixtures increased. The decrease in water absorption may be due to the fineness modulus of white quartz sand. The fineness modulus of white quartz sand (M_k < 2.2) is smaller than that of river sand (M_k = 3.0), which leads to a decrease in the total porosity of concrete, thereby increasing the density and strength. The result is a reduction in water absorption of the concrete.

3.3. Investigation of corrosion resistance of concrete exposed to sodium sulfate (Na_2SO_4) attack

To test the sulfate corrosion resistance, seven groups (three samples for each group) of concrete samples (100×100×100 mm cubes) with different white quartz sand contents were prepared. Cube samples were immersed in a 10 % Na_2SO_4 solution, the duration of immersion in sulfate solution was extended to 450 days. The sulfate resistance of concrete mixtures was evaluated by measuring the compressive strength and ultrasonic pulse velocity test of immersed cubes samples at the age of 450 days. The results of testing concrete samples of developed compositions placed in 10 % Na_2SO_4 solution for a period of 450 days for tests on weight loss and compressive strength are presented in Fig. 8.

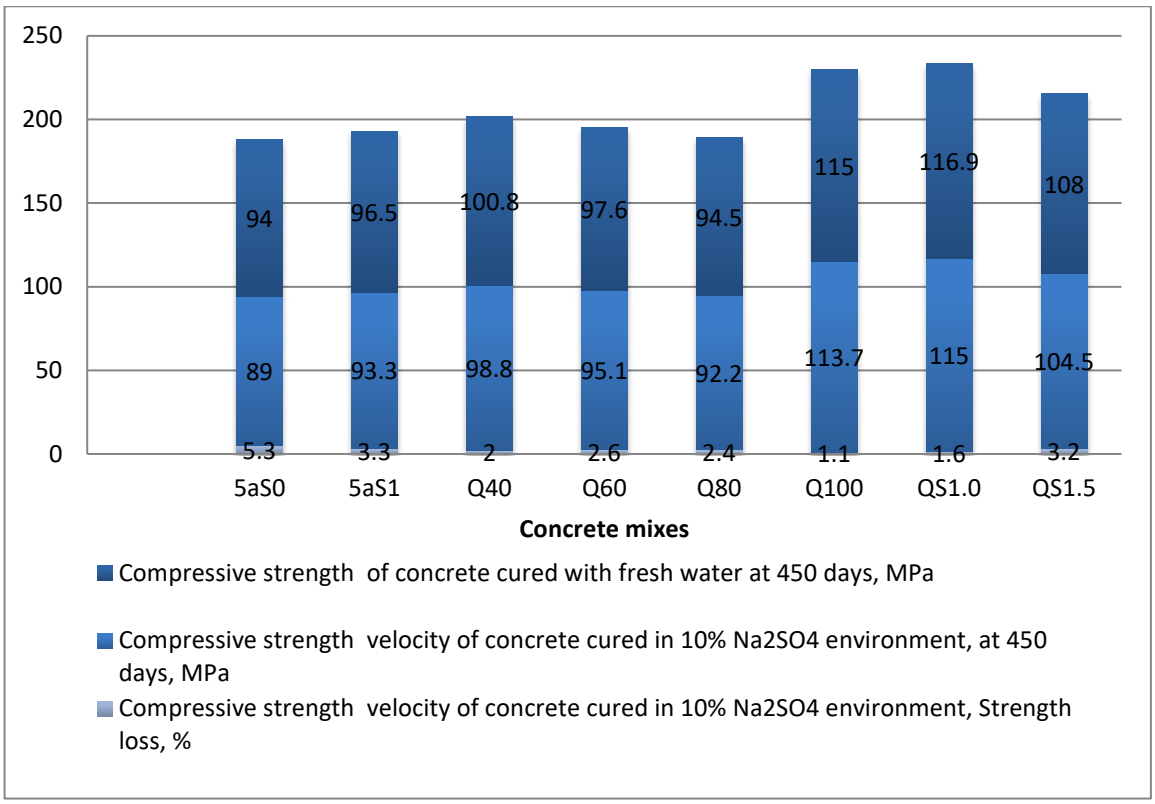

Figure 8. Compressive strength of hardened concrete in various environments.

The test results showed that the presence of white quartz sand augments the sulfate resistance of concrete, and this effect raises with an increase in the amount of white quartz sand instead of river sand. At the age of 450 days, strength tests sample No. 5aS0 showed a reduction in compressive strength by 5.3% due to sulfate corrosion. Mixtures containing white quartz sand showed a low reduction in compressive strength compared to the reference samples, namely, No. Q40, No. Q60, No. Q80, and No. Q100 showed a decrease in compressive strength by 3.3 %, 2.0 %, 2.6 %, and 2.4 %, respectively. In fact, the control sample No. 5aS0 (containing river sand) showed strength reduction of up to 5.3 %, higher than compared to the remaining samples.

It can be noted that the presence of Nano-SiO_2 increases the sulfate resistance of concrete mixture containing 100 % white quartz sand from 1.0 % (No. QS1.0) to 0.9 % (No. QS1.5) compared to the reference sample No. Q100; while compressive strength in the presence of nano-SiO_2 with 1 % content in the concrete mixture containing 100 % river sand (No. 5aS1 mixtures) went by 3.2 % at the age of 450 days.

From the above it follows that adding nano-silica (SiO_2) into concrete mixture intensifies the durability of concretes exposed to external sulfates attack (sulfate corrosion). Sulfate corrosion causes significant expansion and weight loss at the later stage of development, which exposes concrete structures to great danger, especially monolithic concrete structures. Sulfate diffusion in concrete without nano-SiO_2 content occurs at a faster rate, compared to concrete containing nano-SiO_2 in an amount of 1 % by weight of cement, due to the faster development of cracks in concrete.

The results of the conducted experimental studies on the possibility of using local raw materials to create modifying additives, through the use of which it is possible to obtain concretes with high performance and corrosion resistance in contact with an aqueous medium, are consistent with the results of other researchers [31–38].

4. Conclusions

1. We developed compositions of corrosion-resistant concrete with high strength characteristics and low water absorption for underground structures in coastal zone.
2. The developed physical and mathematical model displays the mass transfer of Ca^{2+} ions in the “concrete structure – moist soil – seawater area” system, which makes it possible to control mass transfer processes in order to counteract the corrosion of concrete in coastal underground structures periodically flooded with seawater, and thereby predict their operational durability.

References

1. Gong, J., Jian Cao, Y. Effects of sulfate attack and dry-wet circulation on creep of fly-ash slag concrete. Construction and Building Materials. 2016. 125. Pp. 12–20. DOI: 10.1016/j.conbuildmat.2016.08.023
2. Li, C., Qing, C., Wang, R., Wu, M., Jiang, Z. Corrosion assessment of reinforced concrete structures exposed to chloride environments in underground tunnels: Theoretical insights and practical data interpretations. Cement and Concrete Composites. 2020. 103652. DOI: 10.1016/j.cemconcomp.2020.103652
3. Alexander, M., Beushausen, H. Durability, service life prediction, and modelling for reinforced concrete structures – Review and critique. Cement and Concrete Research. 2019. 122. Pp. 17–29. DOI: 10.1016/j.cemconres.2019.04.018
4. Wenjun, Z., Raoul, F. Corrosion of the reinforcement and its influence on the residual structural performance of a 26-year-old corroded RC beam. Construction and Building Materials. 2014. 51(31). Pp. 461–472. DOI: 10.1016/j.conbuildmat.2013.11.015
5. Wenjun, Z., Raoul, F., Coronelli, D, Cleland, D. Effect of corrosion of reinforcement on the mechanical behaviour of highly corroded RC beams. Engineering Structures. 2013. 56. Pp. 544–554. DOI: 10.1016/j.engstruct.2013.04.017
6. Bonić, Z., Ćurčić, G.T., Trivunić, M., Davidović, N., Vatin, N. Some methods of protection of concrete and reinforcment of reinforced-concrete foundations exposed to environmental impacts. Procedia Engineering. 2015. 117. Pp. 419–430. DOI: 10.1016/j.proeng.2015.08.189
7. Zhao, Y., Jin, W. Damage analysis and cracking model of reinforced concrete structures with rebar corrosion. Steel Corrosion-Induced Concrete Cracking. 2016. Pp. 55–77. DOI: 10.1016/b978-0-12-809197-5.00004-9
8. Aleksandrova, O.V., Quang, N.D., Bulgakov, V.I., Lukyanova, S.V., Petropavlovskaya, V.B. The Effect of Mineral Admixtures and Fine Aggregates on the Characteristics of High-Strength Fiber-Reinforced Concrete. Materials. 2022. 15. 8851. DOI: 10.3390/ma15248851
9. Lu, B.T., Luo, J.L. Synergism of electrochemical and mechanical factors in erosion-corrosion. The Journal of Physical Chemistry B. 2006. 110 (9). Pp. 4217–4231. DOI: 10.1021/jp051985f
10. Zhang, H. Durability reliability analysis for corroding concrete structures under uncertainty. Mechanical Systems and Signal Processing. 2018. 101. Pp. 26–37. DOI: 10.1016/j.ymssp.2017.08.027
11. Rahman, M.A., Zhao, Q., Wiederhold, H. Coastal groundwater systems: mapping chloride distribution from borehole and geophysical data. Grundwasser-Zeitschrift der Fachsektion Hydrogeologie. 2021. 26. Pp. 191–206. DOI: 10.1007/s00767-021-00475-1
12. Crossland, C.J., Kremer, H.H., Lindeboom, H., Crossland, J.I.M., Le Tissier, M.D. Coastal fluxes in the anthropocene: The land-ocean interactions in the coastal zone project of the international geosphere-biosphere programme. Springer Science and Business Media, Berlin, 2005. 253 p.
13. McGranahan, G., Balk, D., Anderson, B. The rising tide: assessing the risks of climate change and human settlements in low elevation coastal zones. Environment and Urbanization. 2007. 19 (1). Pp. 17–37. DOI: 10.1177/0956247807076960
14. Taniguchi, M., Dulai, H., Burnett et al, K.M. Submarine groundwater discharge: Updates on its measurement techniques, geophysical drivers, magnitudes, and effects. Frontiers in Environmental Science. 2019. 75 p. DOI: 10.3389/fenvs.2019.00141
15. Purwoarminta, A., Moosdorf, N., Delinom, R. M. Investigation of groundwater-seawater interactions: A review. IOP Conference Series: Earth and Environmental Science. 2018. 118. 012017. DOI: 10.1088/1755-1315/118/1/012017
16. Bear, J., Cheng, AH-D., Sorek, S., Ouazar, D., Herrebra, I., eds. Geochemical investigation. Seawater intrusion in coastal aquifers – concepts, methods and practices. Kluwer Academic Publishers. Springer Science & Business Media. 1999. 627 p.
17. Barlow, P.M. Ground water in freshwater-saltwater environments of the atlantic coast. US Department of the Interior, USGS, Reston, VA, 2003. 113 p. DOI: 10.3133/cir1262
18. Xiao, H., Tang, Y., Li, H., Zhang, L., Ngo-Duc, T., Chen, D., Tang, Q. Saltwater intrusion into groundwater systems in the Mekong Delta and links to global change. Advances in Climate Change Research. 2021. 12(3). Pp. 342–352. DOI: 10.1016/j.accre.2021.04.005
19. Tran, D.A., Tsujimura, M., Vo, L.P., Nguyen, V.T., Kambuku, D., Dang, T.D. Hydrogeochemical characteristics of a multi-layered coastalaquifer system in the Mekong Delta, Vietnam. Environmental Geochemistry and Health. 2019. 42(2). Pp. 661–680. DOI: 10.1007/s10653-019-00400-9
20. In, K.J., Jiang, Y.R., Jung, S.H., Lee, M.K., Yoo, S.W., Oh, B.H. Durability of concrete under combined exposure conditions of chlorides and sulfates. Key Engineering Materials. 2016. 711. Pp. 319–326. DOI: 10.4028/www.scientific.net/KEM.711.319
21. Hai, D.L. Urban underground space planning. Vietnam Architecture Magazine. Construction Newspaper. 2021.
22. Aggarwal, P. Self-Compacting Concrete: Materials, Properties and Applications Carbonation and corrosion of SCC. Woodhead Publishing Series in Civil and Structural Engineering. 2020. Pp. 147–193. DOI: 10.1016/B978-0-12-817369-5.00007-6
23. Alonso, M.C., Villar, K., Qvaeschning, D., Irico, S., Pérez, G. Investigation on the Combined Interaction of Sulphate and Acidic Attack on Concretes Exposed to Aggressive Environments. In: Menéndez, E., Baroghel-Bouny, V. (eds) External Sulphate Attack – Field Aspects and Lab Tests. RILEM Bookseries. 2020. 21. Springer, Cham. DOI: 10.1007/978-3-030-20331-3_3
24. Yang, W., Baji, H., Li, C.Q. Time-dependent reliability method for service life prediction of reinforced concrete shield metro tunnels. Structure and Infrastructure Engineering. 2017. 08. Pp. 1095–1107. DOI: 10.1080/15732479.2017.1401094
25. Ngo, L.T.Q., Wang, Y.R., Chen, Y.M. Applying Adaptive Neural Fuzzy Inference System to Improve Concrete Strength Estimation in Ultrasonic Pulse Velocity Tests. Advances in Civil Engineering. 2018. 2451915. DOI: 10.1155/2018/2451915
26. Nguyen, L.D., Nguyen, T.V.K., Nguyen, D.V., Tran, A.T., Nguyen, H.T., Heidbüchel, I., Merz, B., Apel, H. Groundwater dynamics in the Vietnamese Mekong Delta: Trends, memory effects, and response times. Journal of Hydrology: Regional. 2021. 33. 100746. DOI: 10.1016/j.ejrh.2020.100746
27. Sato, H., Shibasaki, N., Lap, N.V., Oanh, T.T.K., Lan, N.T.M. Characteristics on distribution of chemical composition in groundwater along the Mekong and Bassac (Hậu) river, Vietnam. Vietnam Journal of Earth Sciences. 2019. 41 (3). Pp. 272–288. DOI: 10.15625/0866-7187/41/3/13969
28. Fedosov, S.V., Rumyanceva, V.E., Kas'yanenko, N.S. Mathematical modeling of mass transfer in the processes of concrete corrosion of the second type. Stroitel'nye materialy. 2008. 7. Pp. 35–39.
29. Fedosov, S.V., Aleksandrova, O.V., Fedoseev, V.N., Loginova, S.A., Nguyen, D.V.Q. Physico-mechanical foundations of theoretical and engineering investigation on the development to corrosion-resistant materials in buried structures of coastal zones.

«XXX Russian-Polish-Slovak Seminar Theoretical Foundation of Civil Engineering». Solid State. 2022. 329. Pp. 209–261. DOI: 10.4028/p-tkq4eg

30. Sorochinsky, V.F. The influence of convective drying on the change of Kirpichev mass-exchange criterion. Journal of Physics: Conference Series. 2019. 1399. 022012. DOI: 10.1088/1742-6596/1399/2/022012
31. Sinsiri, T.T., Jaturapitakkul, P.C., Kiattikomol, K. Effect of finenesses of fly ash on expansion of mortars in mangnesium sulfate. Science Asia. 2006. 32. Pp. 63–69.
32. Aghabaglou, A.M., Inan, G., Sezer, K. Ramyar Comparison of fly ash, silica fume and metakaolin from mechanical properties and durability performance of mortar mixtures view point. Construction and Building Materials. 2014. 70. Pp. 17–25.
33. Mohamed, A.M., Influence of nano materials on flexural behavior and compressive strength of concrete. HBRC Journal. 2016. 12(2). Pp. 212–225. DOI: 10.1016/j.hbrcj.2014.11.006
34. Said, A.M., Zeidan, M.S., Bassuoni, M., Tian, Y. Properties of concrete incorporating nano-silica. Construction and Building Materials. 2012. 36. Pp. 838–844.
35. Hou, P., Qian, J., Cheng, X., Shah, S.P. Effects of the pozzolanic reactivity of nano-SiO2 on cement-based materials. Cement and Concrete Composites. 2015. 55. Pp. 250–258.
36. Sahoo, S., Das, B.B., Rath, A.K., Kar, B.B. Acid, alkali and chloride resistance of high-volume fly ash concrete. Indian Journal of Science and Technology. 2015. 8(19). 72266. DOI: 10.17485/ijst/2015/v8i19/72266
37. Sounthararajan, V.M., Srinivasan, K., Sivakumar, A. Micro filler effects of silica-fume on the setting and hardened properties of concrete. Research Journal of Applied Sciences, Engineering and Technology. 2013. 6(14). Pp. 2649–2654.
38. Mostafa, J., Alireza, P., Omid, F.H., Davoud, J. Comparative study on effects of Class F fly ash, nano silica and silica fume on properties of high performance self-compacting concrete. Construction and Building Materials. 2015. 94. Pp. 90–104.

Contacts:

Sergey Fedosov, *Doctor of Technical Sciences*
ORCID: https://orcid.org/0000-0001-6117-7529
E-mail: fedosovsv@mgsu.ru

Olga Aleksandrova, *PhD Technical Sciences*
ORCID: https://orcid.org/0000-0003-1791-8515
E-mail: aleks_olvl@mail.ru

Boris Bulgakov, *PhD Technical Sciences*
ORCID: https://orcid.org/0000-0002-4737-8524
E-mail: fakultetst@mail.ru

Nadezhda Lukyanova, *PhD Technical Sciences*
ORCID: https://orcid.org/0000-0001-7950-3003
E-mail: galcevanadezda@mail.ru

Quang Nguyen Duc Vinh, *PhD Technical Sciences*
ORCID: https://orcid.org/0000-0001-5840-5279
E-mail: ndvquang@hueuni.edu.vn

Received 24.10.2022. Approved after reviewing 20.02.2024. Accepted 13.03.2024.